Sixth International Symposium on Turbulence and Shear Flow Phenomena
Seoul, Korea, 22-24 June 2009

ANALYSIS OF THE NON-LINEAR DYNAMICS OF A 3-D TRANSITIONAL LID-DRIVEN CAVITY

Thomas Coppin, Jérèmie Chicheportiche, Xavier Gloerfelt & Jean-Christophe Robinet
SINUMEF Laboratory
Arts et Métiers ParisTech
151, boulevard de l'Hôpital, 75013 Paris, France.
xavier.gloerfelt@paris.ensam.fr

ABSTRACT

The dynamics of the viscous flow inside a lid-driven cavity is investigated. The modes predicted by a global linear stability analysis are compared to the results of a direct numerical simulations (DNS). For a 2-D cavity, the successive Hopf bifurcations are in fair agreement with the theoretical predictions, although nonlinear energy tranfers can modify the hierarchy of the peak frequencies. For a 3-D case with periodic spanwise conditions, centrifugal instabilities can occur. The first bifurcation toward a steady state with Taylor-Görtler-Like vortices is well reproduced. However, the base flow then becomes highly three-dimensional, and the dynamics observed in the nonlinear DNS departs from the stability prediction. At Re=1000, based on the unitary length of the cavity, the steady mode persist, and the transition toward an unsteady state is delayed as the Reynolds number is further increased.

INTRODUCTION

The growing literature about cavity flows evidenced a significant interaction between the external flow and the recirculating flow inside the cavity. At moderate Reynolds numbers ($5000 \leq Re \leq 30\,000$), Taylor-Görtler-like (TGL) vortices, originating from the curvature of the main recirculating eddy are identifiable. Their unsteadiness can be responsible of low-frequency modulations of the shear layer/corner interaction, as noted in the experiments of Neary and Stephanoff (1987), or in the simulations of Brès and Colonius (2008).

It is the aim of the present study to investigate separately the dynamics of the viscous flow inside the cavity. The lid-driven cavity problem, which is the flow inside a cavity driven by a translating wall, constitutes an epitome of such flows. The birth of instabilities and their nonlinear evolution as the Reynolds number is increased are studied by using global linear stability theory and direct numerical simulations (DNS). The problem is of course largely dependent on the cavity geometry, but it is thought that the features of the particular aspect ratio retained in the present work can help to shed light on the scenario leading to the transition toward an unsteady and further turbulent state. A square cross-section cavity is studied with periodic boundary conditions in the direction transverse to the lid. The spanwise extent is throughout denoted $\Lambda = 2\pi/\beta$, where β is the transverse wavenumber. The use of periodic conditions is motivated firstly by the possibility to compare the primary instabilities with a global linear stability analysis. The global theory proves to be a powerful tool to study strongly non-parallel flows like the lid-driven cavity (Theofilis et al. 2004). Due to storage limitations of the matrix of the resulting eigenvalue problem, the theory is often restricted to two-dimensional base flows. The three-dimensional perturbation is then assumed periodic in the third direction. Analysis of fully 3-D base flows is only in its infancy, but promises to provide new informations on the secondary bifurcations, or when endwalls are present. The second interest of using periodic conditions is precisely to cope with the increased complexity arising from the blocking action of endwalls. For low Reynolds numbers, these endwalls induce a quick destabilization of the steady flow toward an unsteady one. Three-dimensional elongated TGL structures developing along the edge boundary of the primary eddy are identified in the pioneering experiments of Koseff and Street (1984), and they are triggered by the curvature of the primary eddy resulting from the motion of the lid. The no-slip endwalls induce a pressure gradient, and thus a spanwise velocity. The fluid particles spiraling toward the endwall tend to be pulled into the primary core by the upstream corner vortex, and then spiral monotonically toward the symmetry plane. The collision of the two flow streams in opposite directions at the symmetry plane provides a means of destabilizing the flow (Chiang and Sheu 1998) (Ekman pumping). The influence of the endwalls can thus dominate the dynamics for small spanwise extents (most of the available results used $\Lambda \leq 3$). Even for large extent ($\Lambda = 6.55$), Albensoeder and Kuhlmann (2006) found that the bulk-flow instability has a considerable influence, and that the TGL vortices can exist only within a certain distance from the endwalls. Comparisons between experimental data and numerical results for impulsively started flows in a 3-D lid-driven cavity of aspect ratio 1:1:2 at Reynolds number 1000 by Guermond et al. (2002) indicate the great sensitivity of the transient flow on the spanwise boundary geometry. Since the present investigation focuses on the onset and development of the centrifugal instabilities, spanwise periodic conditions allow to suppress the role of the endwalls. The conditions of the onset of TGL vortices are then investigated for different spanwise aspect ratios, and increasing Reynolds numbers. Another interest of the confined character of the flow is to reduce the non-normality of the global modes, as demonstrated by the study of the transient growth for an optimal perturbation. This point favors the confrontation with asymptotic linear stability results, and thus the analysis of the nonlinear effects.

In the first part of the paper, the numerical methods for the incompressible DNS solver and for the global stability code are detailed. The dynamics for β=0, corresponding to the two-dimensional limit is summarized in a second part, in order to underline the great difference with non-zero β. Three-dimensional centrifugal instabilities are then possible and evolve in the form of nonlinear TGL structures, as described in the third section for a cubical cavity ($\beta = 2\pi$) at Re=1000. The flow bifurcates toward a steady mode, which is predicted by the linear stability analysis. The effect of

varying the spanwise wavenumber is briefly entered upon in the fourth section, where the particular case $\beta = 7$ is seen to lead an oscillatory state, where two spanwise wavelengthes are competitive. The laminar/turbulent transition is investigated in the last part as the Reynolds number is increased.

ANALYSIS TOOLS

DNS solver

The 3D incompressible Navier-Stokes equations are solved in dimensionless form. Since the velocity-pressure formulation is retained, the strategy to be adopted is either grid staggering or collocation to store working variables. Since central differencing is used, we favor the first strategy to avoid grid-to-grid oscillations. Spatial discretisation of nonlinear terms are performed with a compact six-order finite difference scheme with coefficients calculated for a non-uniform Cartesian staggered grid. Viscous terms are discretized with second-order accuracy in space and integrated in time with a second-order implicit Crank-Nicolson, requiring the solution of a linear algebraic system with a block-tridiagonal matrix. Other terms are advanced with a third-order Adams-Bashforth scheme leading to a classical semi-implicit method. Interpolation between node and vertex grids is a crucial step performed with six-order Lagrange interpolation on a non-uniform grid. The satisfaction of discrete divergence-free velocities is enforced by a projection method (Brown et al. 2001) ensuring second-order accuracy in time for both velocity and pressure. The solution of the Poisson pressure equation is obtained at each timestep with a direct solver taking benefit of the block-tridiagonal structure of the matrix for this system. To alleviate the singularity of the Poisson system with four Neumann conditions, a regularization is performed at the last step of the Thomas algorithm. The spanwise boundary conditions of the cavity are periodic, thus, a spectral collocation based on a Fourier decomposition is used in the spanwise direction.

Global linear stability analysis

The proposed stability analysis is based on the classical perturbation technique where the instantaneous flow $\mathbf{q} = (u, v, w, p)^t$ is the superimposition of unknown fluctuations $\hat{\mathbf{q}}$ on a given 2D steady basic flow $\bar{\mathbf{Q}}$: $\mathbf{q}(x, y, z, t) = \bar{\mathbf{Q}}(x, y) + \epsilon\hat{\mathbf{q}}(x, y)$ where $\epsilon \ll 1$ and $\hat{\mathbf{q}}(x, y) = \tilde{\mathbf{q}}(x, y)\exp(i(\beta z - \omega t)) + \textit{complex conjugate}$. The perturbation is then non-homogeneous in the x- and y-directions. Since a temporal approach is adopted, the spanwise wavenumber β is a real parameter, whereas the global circular frequency is the unknown complex number $\omega = \omega_r + i\omega_i$. After introducing this decomposition in the dimensionless 3D incompressible Navier-Stokes equations, a linearization leads to the following equations:

$$\frac{\Delta_2\tilde{u}}{Re} - \bar{U}\frac{\partial\tilde{u}}{\partial x} - \frac{\partial\tilde{p}}{\partial x} - \bar{V}\frac{\partial\tilde{u}}{\partial y} - (\frac{\beta^2}{Re} + \frac{\partial\bar{U}}{\partial x})\tilde{u} - \frac{\partial\bar{U}}{\partial y}\tilde{v} = -i\omega\tilde{u}$$

$$\frac{\Delta_2\tilde{v}}{Re} - \bar{U}\frac{\partial\tilde{v}}{\partial x} - \frac{\partial\tilde{p}}{\partial y} - \bar{V}\frac{\partial\tilde{v}}{\partial y} - (\frac{\beta^2}{Re} + \frac{\partial\bar{V}}{\partial y})\tilde{v} - \frac{\partial\bar{V}}{\partial x}\tilde{u} = -i\omega\tilde{v}$$

$$\frac{\Delta_2\tilde{w}}{Re} - \bar{U}\frac{\partial\tilde{w}}{\partial x} - i\beta\tilde{p} - \bar{V}\frac{\partial\tilde{w}}{\partial y} - \frac{\beta^2}{Re}\tilde{w} = -i\omega\tilde{w}$$

$$\frac{\partial\tilde{u}}{\partial x} + \frac{\partial\tilde{v}}{\partial y} + i\beta\tilde{w} = 0$$

where $\Delta_2 = \partial^2/\partial x^2 + \partial^2/\partial y^2$. These equations can be written as a complex non-symmetric generalized eigenproblem, with eigenvalue ω and eigenvector $\tilde{\mathbf{q}}$: $[A(Re, \beta) - \omega B(Re, \beta)]\tilde{\mathbf{q}} = 0$. The problem is discretized on a non uniform Cartesian grid refined near the walls. A finite-difference scheme, optimized in the wavenumber space, along with a coordinate transform are used to evaluate the first and second derivatives (Merle et al. 2007). Lastly, the eigenvalue problem is solved with an Implicitly Restarted Arnoldi Method (Lehoucq et al. 1997). As a result, the imaginary and real parts of ω pertain respectively to the growth/damping rate and the frequency of an instability mode. If $\omega_i < 0$ the perturbation decreases in time so the flow is stable, whereas if $\omega_i > 0$ the flow is unstable.

DYNAMICS OF THE CAVITY FOR β=0

The case β=0 corresponds to the two-dimensional lid-driven cavity flow. Numerous papers deal with the determination of the critical Reynolds number for the first Hopf bifurcation toward an unsteady state for 2-D cavity flow. Even if a value of Re_c=8000 is probable from these studies, a scatter is still noticeable for the precise values of Re_c : 7763 in Poliashenko and Aidun (1995), 7998 in Fortin et al. (1997), 7972 in Cazemier et al. (1998), 8018 in Auteri et al. (2002), 8375 in Tiesinga et al. (2002), 7400 in Peng et al. (2003), 8031 in Sahin and Owens (2003), 8000 in Abouhamza and Pierre (2003), or between 8000 and 8050 in Bruneau and Saad (2006). Re_c depends on the method (bifurcation analysis in Poliashenko and Aidun (1995), Tiesinga et al. (2002), reduced-order model in Cazemier et al. (1998), stability analysis in Sahin and Owens (2003), Abouhamza and Pierre (2003), DNS in Auteri et al. (2002), Peng et al. (2003), Bruneau and Saad (2006)), on the spatial discretization as shown in Gervais et al. (1997), or on the time integration algorithm in Bruneau and Saad (2006). In the present study, the critical Reynolds number is predicted to be 8035 from a global stability analysis with a 150^2 grid. A value of 7865 is estimated with a $\sqrt{Re - Re_c}$ fitting from the DNS kinetic energy growth with a 126^2 grid. A value of 7974 in closer agreement with the preceding references is obtained for a 250^2 grid. After the first bifurcation, a periodic flow with the frequency of 0.44 is obtained. The perturbation field from the DNS, depicted in figure 1, is in excellent agreement with the stability eigenfunction for the most unstable mode, and indicates that Kelvin-Helmholtz-like instabilities develop along the dividing streamline $\Psi = 0$.

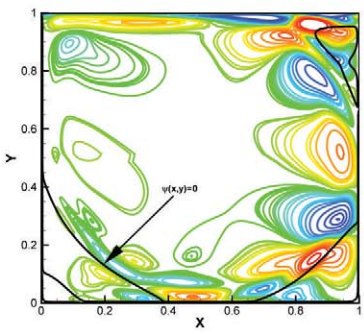

Figure 1: U-velocity perturbations for the DNS at Re=7900 (flow is from right to left).

When the Reynolds number is further increased, a sequence of successive Hopf bifurcations is observed. The most unstable frequencies and the successive critical Reynolds

Table 1: Critical Reynolds numbers Re_c, and most unstable frequencies for the first five Hopf bifurcations predicted by the global linear stability analysis with a 150^2 point grid.

Re_c	8135	8731	9054	9135	10129	
	0.446	0.445	0.617	0.617	0.617	+
$\omega_r/2\pi$	-	0.617	0.441	0.438	0.710	↑
Stab.	-	-	0.534	0.534	0.431	ω_i
	-	-	-	0.715	0.530	↑
	-	-	-	-	0.766	-

Table 2: Principal "linear" peak frequencies obtained for a 250^2 point grid DNS for increasing Reynolds numbers.

Re	8000	8500	9000	10000
	0.45	0.445	0.442	0.617
$\omega_r/2\pi$	-	-	0.618	0.436
DNS	-	-	0.534	0.52
	-	-	-	0.70

number predicted by the global linear theory are given in table 1. They are in fair agreement with the principal peaks observed in the DNS velocity spectra, reported in table 2. Only the "linear" frequencies are given, meaning that the harmonics and interaction frequencies due to the nonlinear effects are discarded.

The comparison for a relatively high Reynolds number Re= 10^4 indicates that, in the case β=0, the global linear theory can help interpreting the dynamics of the cavity flow. The basic flow for Re= 10^4 is indeed depicted in figure 2. A large primary eddy and three secondary eddies located near the cavity corners are visible. The global stability approach shows that this quasi-periodic state corresponds to four unstable modes (f_1=0.61, f_2=0.71, f_3=0.44 and f_4=0.53) in the spectrum of figure 2. DNS simulations exhibit similar "linear" frequencies (table 2), although the hierarchy between the peaks is slighly modified. The frequency 0.44 remains for instance the second most unstable mode due to nonlinearities. Moreover, some nonlinear self-interactions of unstable modes are observed, which generate harmonics and nonlinear mutual interactions of modes ($f_i \pm f_j$, nf_j, ... with $(i,j) \in [1,...,4]$ and $n \in$ N). An important energy transfer is induced between some characteristic scales.

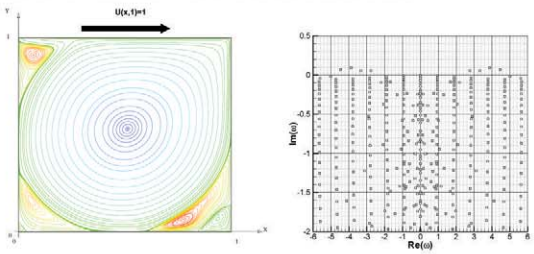

Figure 2: Basic flow for the streamline function at Re=10^4 on the left, and eigenvalues spectrum at Re=10^4 from the global stability analysis.

Therefore, as the temporal complexity of the flow increases in this sequence of bifurcations when Re increases, the spatial complexity increases as well. Motions occur on smaller length scales and on a broader range of length scales. When the Reynolds number is still increased, a tendency toward a reduction of the number of spectral peaks is observed, reminding an inverse cascade of energy characteristic of two-dimensional flows.

COMPARISON OF GLOBAL STABILITY AND 3-D DNS FOR A SQUARE CAVITY AT RE = 1000

The nature of the cavity instabilities are very different when a 3-D flow with spanwise periodic conditions is considered ($\beta \neq 0$). Centrifugal instabilities can occur for a critical Reynolds number Re_c one order of magnitude smaller. The neutral curves for the four least-stable instability modes are depicted in figure 3. They represent the limit of stability of a mode in the parameter space (Re, β). The first critical Reynolds number $Re_c \simeq 780$, for $\beta \simeq 15$, is associated with a steady mode, thereafter referred to as the S1 mode. The unsteady modes, referred to as the travelling modes T1, T2, T3, become unstable respectively for $(Re_c, \beta) \simeq (840, 15)$, $(920, 7.5)$, and $(960, 14)$. Note that the corresponding most amplified wavenumber is very close for the S1 and T1 modes, whereas the preferred wavenumber of T2 is well distinct.

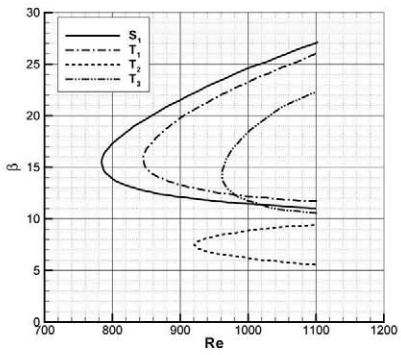

Figure 3: Neutral curves for the first four eigenmodes (grid 125^2).

In their experiments for a square cavity with a spanwise aspect ratio of 3, Benson and Aidun (1992) identify an unsteady flow, whose frequency is very close to the one of T1, as noted by Theofilis et al. (2004). To understand which mode is selected when the effects of endwalls are not taken into account, direct numerical simulations were performed with refined grids (Chicheportiche et al. 2008) for a cubical lid-driven cavity at $Re = 1000$ with periodic conditions in the spanwise direction. The four least-stable instability modes from the global linear theory at this Reynolds number are given in table 3. The four modes S1, T1, T2, T3 are thus potentially unstable. The amplification rate and the frequency of each modes converge with two digits after the decimal point when the grid is refined. Moreover the values are in very good agreement with the work of Theofilis et al. (2004), Albensoeder et al. (2001), Spasov et al. (2003), Non et al. (2006). The DNS calculations are performed for a cubical cavity, *i.e.* with a spanwise extent $\Lambda = 1$, corresponding to $\beta = 2\pi$. The flowfield is validated with the benchmark of Albensoeder and Kuhlmann (2005). A three-dimensional steady Taylor-Görtler-Like flow is observed when periodic spanwise boundary conditions are used.

To confirm that the final non-linear 3-D structures are indeed induced by the S1 instability, the perturbation fields during the linear phase are extracted. For that purpose, the 2-D basic flow is subtracted from instantaneous fields taken at one instant in the middle of the exponential growth

Table 3: Maxima of amplication rate and circular frequency of the first four eigenmodes from the stability analysis, given for 125^2 and 150^2 point grids.

	S1, $\beta = 17.0$		**T1**, $\beta = 17.0$	
$Re = 1000$	ω_i	ω_r	ω_i	ω_r
125^2	0.1422	0.0000	0.0988	0.6967
150^2	0.1430	0.0000	0.0995	0.6971
	T2, $\beta = 7.0$		**T3**, $\beta = 15.0$	
$Re = 1000$	ω_i	ω_r	ω_i	ω_r
125^2	0.0118	0.4962	0.0162	1.3721
150^2	0.0117	0.4966	0.0168	1.3730

phase. The resulting perturbation field is compared to the S1 eigenmode from the stability analysis in figure 4. We observe a great similarity between these fields. Moreover, the S1 mode is clearly a centrifugal instability which is related to TGL vortices. This steady mode dominates the other unsteady unstable modes predicted by the theoretical approach. The level of convergence is quantified by extracting the growth rate ω_i in the exponential growth of w. As the grid is refined, the growth rate from DNS converges toward a value which is very close to the growth rate of the mode S1 for $\beta = 18.85$ (Chicheportiche et al. 2008).

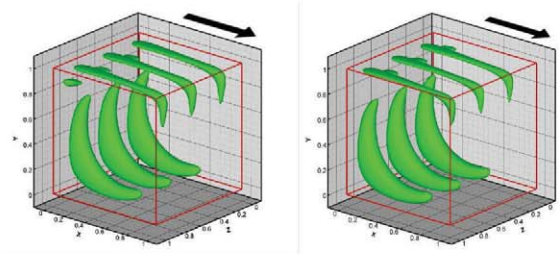

Figure 4: Isocontour of perturbative field for the u-component of velocity from DNS ($100 \times 100 \times 64$ points) on the left, and S1 stability mode ($150 \times 150 \times 44$ points) on the right. The lid motion is indicated by the arrow.

Mode selection in the transverse direction

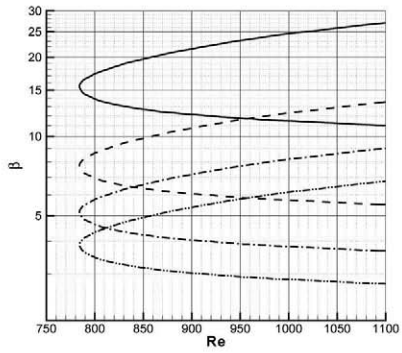

Figure 5: Neutral curves for the S1 mode replicated for different multiple of the critical wavelength $2\pi/k_c$: solid line: $n_{\mathrm{TG}} = 1$ TGL vortex pairs; dashed line: $n_{\mathrm{TG}} = 2$; dash-dotted line: $n_{\mathrm{TG}} = 3$; dash-double-dotted line: $n_{\mathrm{TG}} = 4$.

The spanwise wavenumber is selected by the periodic conditions to be close to a multiple of the wavelength corresponding to the maximal amplification, referred to as the critical wavelength $\lambda_c = 2\pi/k_c$. In the previous configuration where the spanwise dimension is $\Lambda = 1$, this leads to an observed spanwise wavenumber $k_z = 3 \times 2\pi/\Lambda = 18.85$, close to the critical wavenumber $k_c = 17$ (see table 3). This selection mechanism has been described by Albensoeder and Kuhlmann (2006), by varying Λ. A similar study by varying $\beta = 2\pi/\Lambda$ has been conducted with the present DNS solver, and is in fairly good agreement with the results of Albensoeder and Kuhlmann (2006). The neutral curves for the first bifurcation from the 2-D basic flow toward a steady 3-D flow are plotted in figure 5 for a number $n_{\mathrm{TG}} = \{1, 2, 3, 4\}$ of TGL vortex pairs. They are at equally spaced spanwise extent $\Lambda = n_{\mathrm{TG}}\lambda_c$. A logarithmic scale is chosen for the wavenumber since the neutral curves become flatter as n_{TG} increases. When Λ is close to a multiple of the critical wavelength, the bifurcation is supercritical, and follows the linear stability theory. For β corresponding to intersection of the neutral curves, nonlinearities yield a subcritical bifurcation. A possible hysteresis is noted by Albensoeder and Kuhlmann (2006) whether the Reynolds number is increased or decreased. Oscillating flows are observed in these intermediate regions where two multiples of the wavelength are competitive. The topology of one oscillating case, obtained for $\beta = 7$, is investigated. The residual curves, plotted in figure 6, show a low-frequency oscillating pattern. The intermediate flowfields are characterized. For example, 3-D plots of the y-component of the vorticity are presented in figure 7, and indicate a switching between two and three pairs of counterrotating Taylor-Görtler-like vortices.

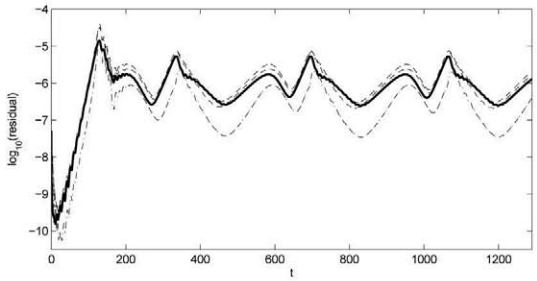

Figure 6: Residuals for the cavity with $\beta = 7$: solid line : w; dashed lines : u and v; dash-dotted line : p.

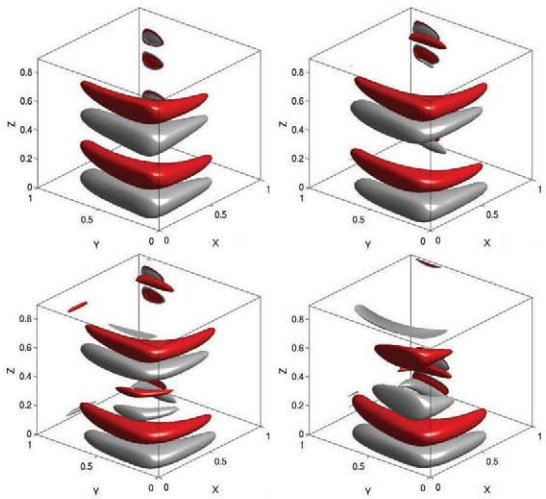

Figure 7: Instantaneous isosurfaces of y-vorticity, $\beta = 7$. From left to right, and top to bottom: $t = 761$, 942, 1019, 1071.

SECOND BIFURCATION TOWARD AN UNSTEADY STATE

The Reynolds number is varied between 700 and 2500, for the square cavity with a fixed transverse dimension $\Lambda = 1$. After a primary bifurcation around to Reynolds number 780 beyond which the flow become three-dimensional and steady, a second bifurcation toward an unsteady state appears between Re=1100 and 1200. This bifurcation is characterized by a frequency near $f_0 \simeq 0.12$. Physically this unsteadiness corresponds to a transverse motion of Taylor-Görtler vortices with a larger amplitude at the edge of the vortex than at its root. After this secondary bifurcation, for higher Reynolds number, the transition process is then very rapid. Some spectra and temporal evolutions for spanwise velocity component w are reproduced in figure 8, and the degree of order is characterized by the phase portraits in figure 9. For $1200 \leq \mathrm{Re} \leq 1300$, the spatial organization shown in figure 4 still remains true on average. At this Reynolds number range, the flow is mainly periodic, with some harmonics noticeable in the spectra, and indicating nonlinear effects. For $\mathrm{Re} > 1300$, a new low frequency appears, $f_1 \simeq 0.053$, and the loop observed in the phase plots are now spreading around the previous limit cycle. When the Reynolds number increases these frequencies interact between them leading to important non-linear coupling. A large degree of randomness is then observed in the time histories of the fluctuations, even if the mean flow structure remains organized (with three pairs of TGL vortices) until Re=1800 (see Fig. 10). The unsteadiness remains located in the vicinity of the TGL structures. The movement is always of pendulum type, with the curved streamwise vortices oscillating back and forth. For higher Reynolds number, $\mathrm{Re} > 1800$, the phase plots are progressively more isotropic whose trajectories eventually no longer be periodic and characteristics of a turbulent state.

CONCLUSIONS

In this investigation, a three-dimensional steady Taylor-Görtler-Like flow is found for a square lid-driven cavity with periodic spanwise boundary conditions. The first bifurcation corresponds to the steady mode S1 of a stability analysis. The mechanism for selection of the number TGL vortex pairs in the spanwise direction is very similar to the results of Albensoeder and Kuhlmann (2006). The oscillating flow observed for β=7 has been detailed, and shows the competition between two spanwise flow arrangement. When the Reynolds number increases, the flow becomes unsteady keeping a large regularity. Some intermittency of the TGL vortex pairs is first noted. The spanwise coherence is then altered by the developing turbulence.

In future work, the second bifurcation will be analyzed by studying the stability of the nonlinear stationary solution of the three-dimensional Navier-Stokes equations. This study requires both the development of a specific algorithm to obtain the base flow and using a direct method of resolution, without matrix, of the eigenvalue problem.

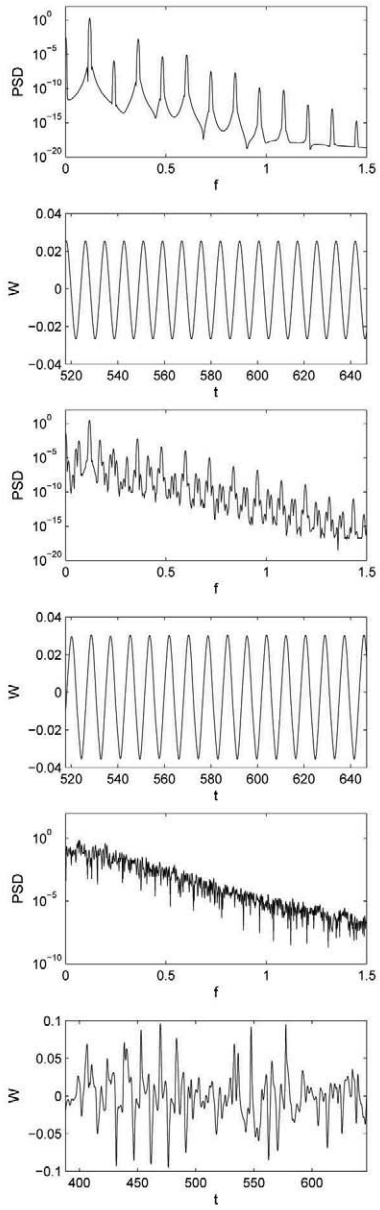

Figure 8: Power spectral density (above) and time histories (below) of W, at point $(1/6; 1/6; 1/2)$. From top to bottom: $Re = 1200$, 1300, and 2000.

REFERENCES

M.D. Neary and K.D. Stephanoff. Shear-layer-driven transition in a rectangular cavity. *Phys. Fluids*, 30(10): 2936–2946, 1987.

G.A. Brès and T. Colonius. Three-dimensional instabilities in compressible flow over open cavities. *J. Fluid Mech.*, 599:309–339, 2008.

V. Theofilis, P.W. Duck, and J. Owen. Viscous linear stability analysis of rectangular duct and cavity flows. *J. Fluid Mech.*, 505:249–286, 2004.

J.R. Koseff and R.L. Street. Visualization studies of a shear driven three-dimensional recirculating flow. *ASME Journal of Fluids Engineering*, 33:594–602, 1984.

T.P. Chiang and R.R. Sheu, W.H.and Hwang. Effect of Reynolds number on the eddy structure in a lid-driven cavity. *Int. J. Numer. Meth. Fluids*, 26:557–579, 1998.

S. Albensoeder and H.C. Kuhlmann. Nonlinear three-dimensional flow in the lid-driven square cavity. *J. Fluid Mech.*, 569:465–480, 2006.

J.-L. Guermond, C. Migeon, G. Pineau, and L. Quartapelle. Start-up flows in a three-dimensional rectangular driven cavity of aspect ratio 1:1:2 at Re = 1000. *J. Fluid Mech.*, 450(169-199), 2002.

D.L. Brown, R. Cortez, and M.L. Minion. Accurate projection method for the incompressible Navier-Sokes equa-

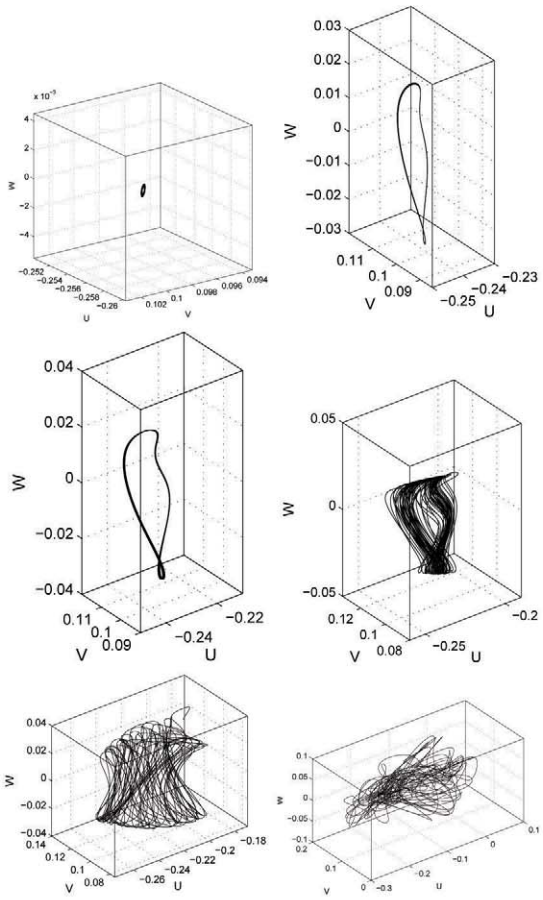

Figure 9: Phase portraits at point (1/6; 1/6; 1/2). From left to right and from top to bottom: Re = 1100, 1200, 1250, 1300, 1350 and 2000.

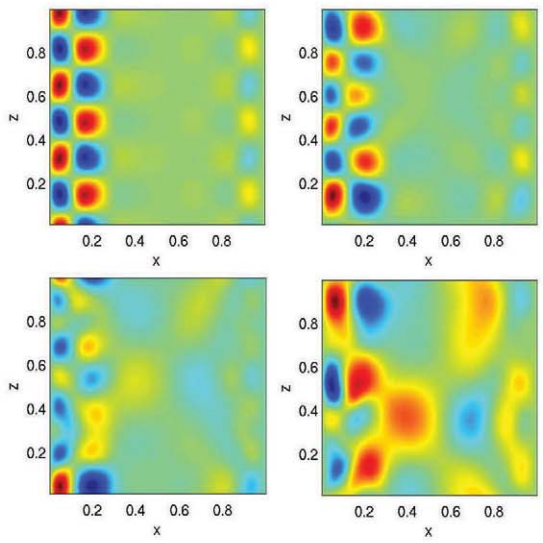

Figure 10: Mean velocity w in the plane $y = 1/2$. From the left to the right and from top to bottom: Re = 1300;1500;1600;1800.

tions. *J. Comput. Phys.*, 168:464–499, 2001.

X. Merle, J.-C. Robinet, and A. Lerat. Efficient numerical method for global linear stability problem. *37th AIAA Fluid Dynamics Conference and Exhibit*, 25-28 June, Miami, Florida, AIAA Paper 2007-, 2007.

R. B. Lehoucq, D.C. Sorensen, and C. Yang. ARPACK user's guide: solution of large scale eigenvalue problems with Implicity Restarted Arnoldi Methods. 1997. http://www.caam.rice.edu/software/ARPACK/.

M. Poliashenko and C.K. Aidun. A direct method for computation of simple bifurcations. *J. Comput. Phys.*, 121: 246–260, 1995.

A. Fortin, M. Jardak, J.J. Gervais, and R. Pierre. Localization of Hopf bifurcations in fluid flow problems. *Int. J. Numer. Meth. Fluids*, 24(1185-1210), 1997.

W. Cazemier, R.W. Verstappen, and A.E. Veldman. Proper orthogonal decomposition and low-dimensional models for driven cavity flows. *Phys. Fluids*, 10(7):1685–1699, 1998.

F. Auteri, N. Parolini, and L. Quartapelle. Numerical investigation on the stability of singular driven cavity flow. *J. Comput. Phys.*, 183:1–25, 2002.

G. Tiesinga, F.W. Wubs, and A.E.P. Veldman. Bifurcation analysis of incompressible flow in a driven cavity by the Newton-Picard method. *Journal of Computational and Applied Mathematics*, 140:751–772, 2002.

Y.-F. Peng, Y.-H. Shiau, and R.R. Hwang. Transition in a 2D lid-driven cavity flow. *Computers and Fluids*, 32: 337–352, 2003.

M. Sahin and R.G. Owens. A novel fully-implicit finite volume method applied to the lid-driven cavity problem - Part II : Linear stability analysis. *Int. J. Numer. Meth. Fluids*, 42:79–88, 2003.

A. Abouhamza and R. Pierre. A neutral stability curve for incompressible flows in a rectangular driven cavity. *Mathematical and Computer Modelling*, 183:1–25, 2003.

C.H. Bruneau and M. Saad. The 2D lid-driven cavity problem revisited. *Computers and Fluids*, 35(3):326–348, 2006.

J.J. Gervais, D. Lemelin, and R. Pierre. Some experiments with the stability analysis of discrete incompressible flows in the lid-driven cavity. *Int. J. Numer. Meth. Fluids*, 24:477–492, 1997.

J.D. Benson and C.K. Aidun. Transition to unsteady nonperiodic state in a through-flow lid-driven cavity. *Phys. Fluids A*, 4(10):2316–2319, 1992.

J. Chicheportiche, X. Merle, X. Gloerfelt, and J.C. Robinet. Direct numerical simulation and global stability analysis of three-dimensional instabilities in a lid-driven cavity. *C. R. Méc., Acad. Sci. Paris*, 336:586–591, 2008.

S. Albensoeder, H.C. Kuhlmann, and H.J. Rath. Three-dimensional centrifugal-flow instabilities in the lid-driven-cavity problem. *Phys. Fluids*, 13(1):121–135, 2001.

Y. Spasov, J. Herrero, F.X. Grau, and F. Giralt. Linear stability analysis and numerical calculations of the lid-driven flow in a toroidally shaped cavity. *Phys. Fluids*, 15(1):134–146, 2003.

E. Non, R. Pierre, and J.-J. Gervais. Linear stability of the three-dimensional lid-driven cavity. *J. Fluid Mech.*, 18: 084103, 2006.

S. Albensoeder and H.C. Kuhlmann. Accurate three-dimensional lid-driven cavity flow. *J. Comput. Phys.*, 206: 536–558, 2005.